

# **Thermal mixing of two miscible fluids in a T-shaped microchannel**

Bin Xu, Teck Neng Wong\*, Nam-Trung Nguyen, Zhizhao Che

School of Mechanical and Aerospace, Nanyang Technological University  
50 Nanyang, Avenue, Singapore 639798

## **Abstract**

This paper presents theoretical and experimental investigations on thermal mixing in the T-shaped microchannel. In the experiments, DI-water with Rhodamine B solution is introduced by syringe pumps to flow side by side in the T-shaped microchannel. External electric fields are used to supply voltage to the thermoelectric modules (TEC) to heat up and cool down the DI-water with Rhodamine solution in the microchannel. The inlet volumetric flow rates of both hot and cold fluids are varied to investigate thermal mixing in the T-shaped microchannel. The fluid temperature field in the T-shaped microchannel is measured using fluorescence imaging technique. The PMMA temperature field is captured by an infrared thermal tracer camera. The temperature distributions under different flow rates are investigated. The results indicate that the Reynolds number is a crucial parameter to the heat transfer process in the microchannel. The effectiveness of thermal mixing is found better at lower Reynolds number. The measured temperature field in the T-shaped microchannel agrees well with the theoretical model.

\*Corresponding author. E-mail: [mtnwong@ntu.edu.sg](mailto:mtnwong@ntu.edu.sg)

## 1. Introduction

Microfluidics has received great attention over past decades. More and more researchers focus on this area because of its compatibility and high performance with analysis (Auroux et al. 2002; Reyes et al. 2002; Wang et al. 2004). Microfluidics shows immense application in many areas such as medical, chemical, biological and so on.

When we conduct various chemical or biological experiment and analysis on microfluidic system, regulating the fluid temperature is very important especially during reaction and separation. A lot of examples such as enzyme-catalyzed reaction on a microchip (Tanaka et al. 2000), isoelectric focusing with thermally generated pH gradient (Huang et al. 2002), polymerase chain reaction (PCR) amplification (Kim et al. 2006) and temperature gradient focusing via Joule heating (Sommer et al. 2007) have manifested the importance of controlling temperature in analytical chemistry and biochemistry. However, controlling of fluid temperature field precisely is very difficult because of the micro-scale of these microchips. Measuring fluid temperature in the microchannel is difficult due to the size limit. There are many ways to measure the internal temperature, including thermochromic solution (Wätzig 1992; Chaudhari 1998), raman spectroscopy (Davis et al. 1993; Liu et al. 1994) and nanoliter-volume proton nuclear magnetic resonance (NMR) spectroscopy (Lacey et al. 2000).

Nowadays, the most popular method for measuring internal fluid temperature field in microchannel is Laser Induced Fluorescence (LIF), which was based on the temperature-dependent fluorescence. In this method, the temperature-dependent fluorescence Rhodamine B was added into the working fluid. The intensity of the fluorescence was imaged using a standard fluorescence microscope and a CCD camera (Ross et al. 2001). The internal fluid temperature field can be obtained by measuring the intensity of fluid through a calibration curve.

Two-fluid flow in microchannel is widely used in the biological experiment and analysis. The Reynolds number ( $Re$ ) is usually very small and the flow is always laminar in microfluidic devices. From the view of mass mixing, laminar fluid

diffusion interface (LFDI) is generated when two-fluid flow in parallel within a microfluidic device (Jandik et al. 2002). Diffusion, which is a function of mass diffusion coefficient and distance, is the only mechanism to determine the mass mixing in the microfluidic device (Kamholz et al. 1999).

For the thermal mixing in the microchannel, the LFDI will be stratified due to the reason that the thermal diffusivity coefficient is 1000 times larger than the mass diffusion coefficient. A Y-shaped microchannel was investigated experimentally (Tomasz Glowinski 2009). Some temperature contour plots were given to show the thermal mixing process. To the best knowledge of the author, theoretical model related to thermal mixing in the microchannel is yet to be reported. In this paper, a theoretical model is proposed for the thermal mixing at the intersection of T-shaped microchannel. This paper attempts to understand and to explain the thermal mixing process in the microscale.

## **2. Experiment**

### *2.1. Fluorescence imaging setup*

The schematic illustration of the fluorescence imaging setup is shown in Fig. 1, consisting of four main components: an illumination system, an optical system, a coupled charge device (CCD) camera and a personal computer (PC) based control system. A mercury lamp with the wave length of 540nm is employed as the illumination source for the fluorescence imaging setup.

The Nikon inverted microscope (Model ECLIPSE TE2000-S) with a set of epi-fluorescent attachments is used as the optical system. Excitation filter, dichroic mirror and emission filter constitute the filter cube. Emission filters are used in the measurements to select the specific emission wavelength of the sample and to remove traces of excitation light.

An interline transfer CCD camera (Sony ICX 084) is used for recording the images. The resolution of the camera is 1324×1024 pixels with 16 bits grayscale. The

active area of the CCD sensor is 4mm×3mm. The exposure time for recording the image is  $7 \times 10^4 \mu s$ .

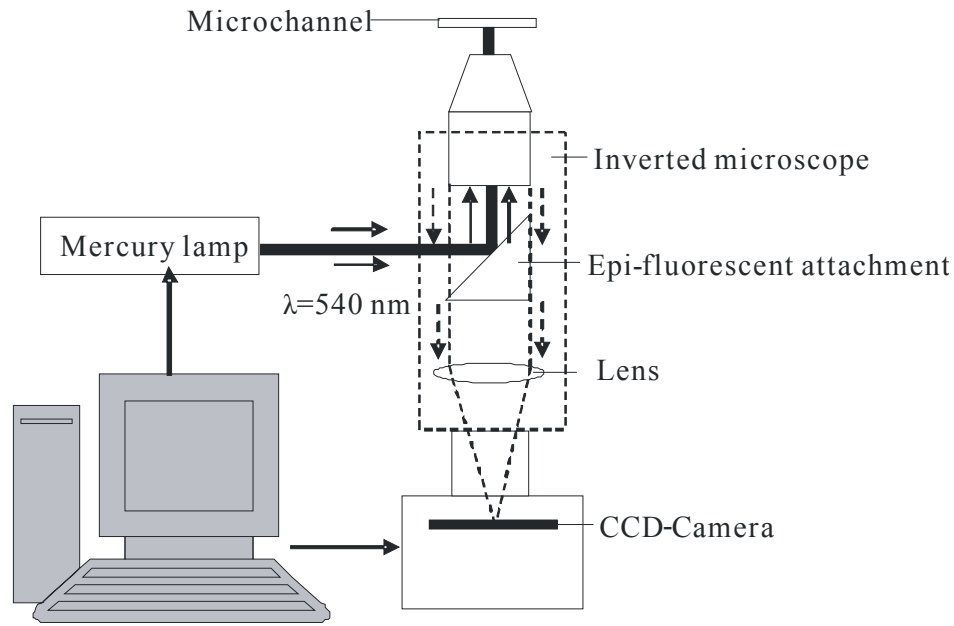


**Fig. 1 Schematic illustration of experimental setup for fluorescence imaging**

## 2.2. Calibration of temperature setup

Fig. 2 shows the layout of the microchannel for the calibration of temperature measurement. The thermal bonding technique is used to bond three polymethylmethacrylate (PMMA) plates (55 mm × 25 mm) together. The channel height is determined by the middle PMMA plate, with a cross section of  $1000 \mu m \times 500 \mu m$ . The channel structures were cut into the middle PMMA plate using CO<sub>2</sub> laser. The thermocouple which was calibrated using Thermal Calibration Cool/Heat Source Model 18B was inserted into the vertical slot in the middle PMMA plate to measure the internal fluid temperature in the microchannel. The dimension of the square groove on the top PMMA plate was 15mm × 15mm.

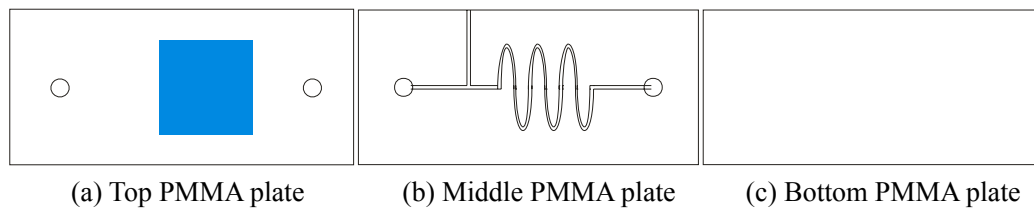
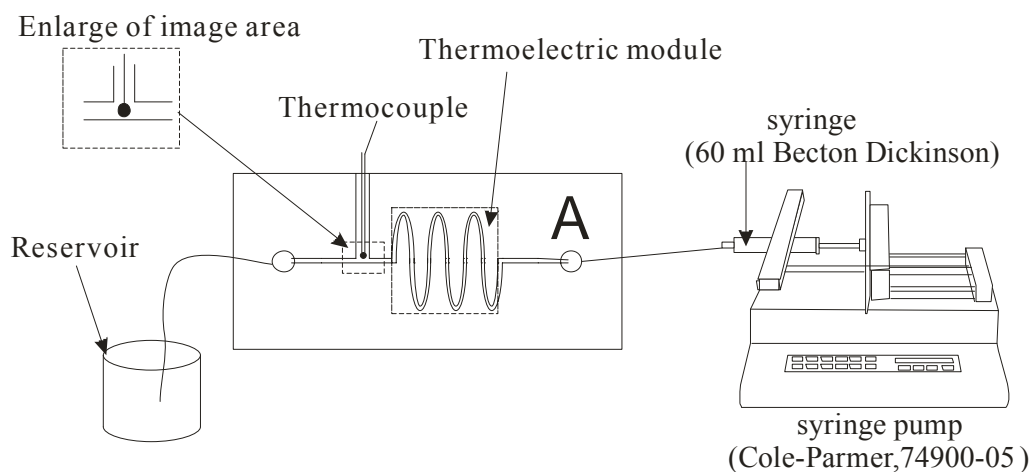


**Fig. 2 Calibration of a chip design**

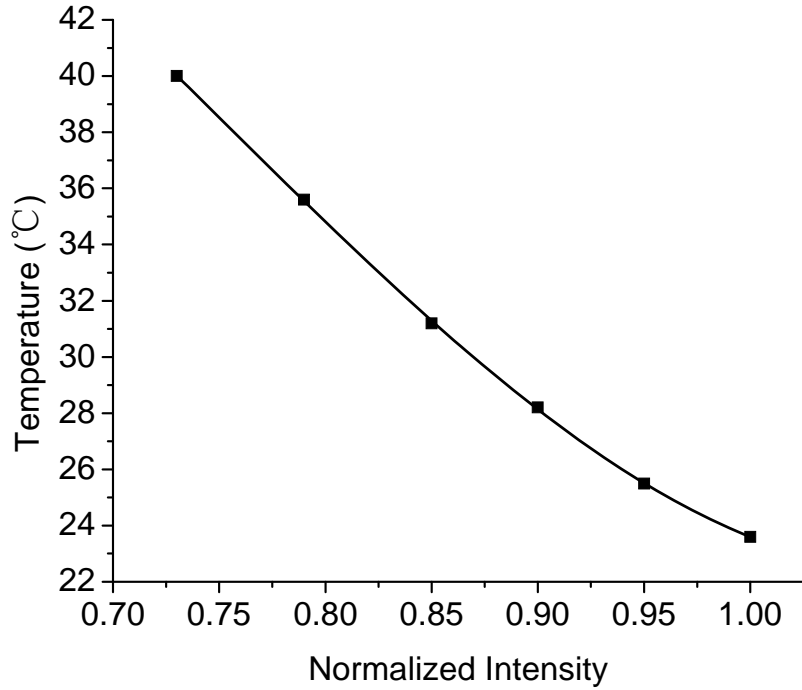
The schematic of the experimental setup for the calibration of temperature measurement is shown in Fig. 3. It is used to determine the relationship between the

fluorescence intensity and temperature. Rhodamine B solution (0.025g/100ml) is introduced into the inlet port A by a single syringe pump (Cole-Parmer, 74900-05, 0.2  $\mu$ l/h to 500 l/h, accuracy of 0.5%). A low voltage power supply (GW Model GPC- 30300) is used to supply voltage to the thermoelectric module (TEC) to heat up the Rhodamine B solution in the microchannel.

The thermoelectric module is put on the square slot on the top PMMA plate to heat the Rhodamine B solution by varying the voltages. The temperature of the solution increases with increasing the voltage. The image of the Rhodamine B solution in the microchannel for different temperature is captured with the microscope. Each captured image is generated by 30 sequential video frames. For the calibration curve, the fluorescence intensity for the image at each temperature is determined by averaging the intensity value (after background subtraction) of all the pixels of the corresponding image. A calibration curve is generated to accurately describe the dependence of Rhodamine B fluorescence on temperature which is shown in Fig. 4.



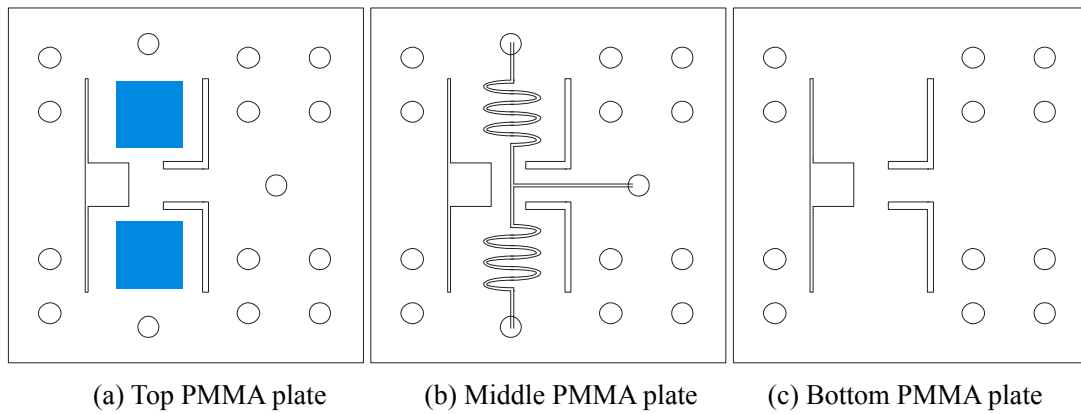
**Fig. 3 Schematic illustration of experimental setup for calibration of temperature**



**Fig. 4 Normalized fluorescence intensity as a function of temperature used to calibrate the fluorescence-based temperature measurement**

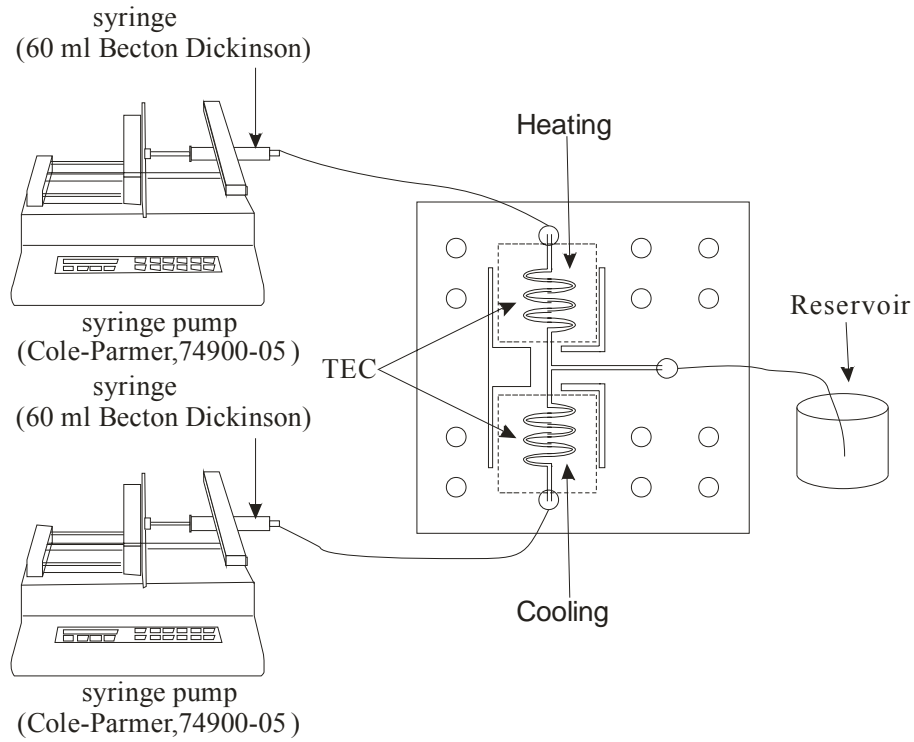
### 2.3. Thermal mixing setup

Fig. 5 shows the layout of the microchannel for the thermal mixing. The thermal bonding technique is used to bond three polymethylmethacrylate (PMMA) plates (50 mm × 50 mm) together. The channel height is determined by the middle PMMA plate, with a cross section of  $1000\mu\text{m} \times 500\mu\text{m}$ . The channel structures were cut into the middle PMMA plate using CO<sub>2</sub> laser. The dimension of the square groove on the top PMMA plate was 9mm × 9mm.



**Fig. 5 Thermal mixing chip design**

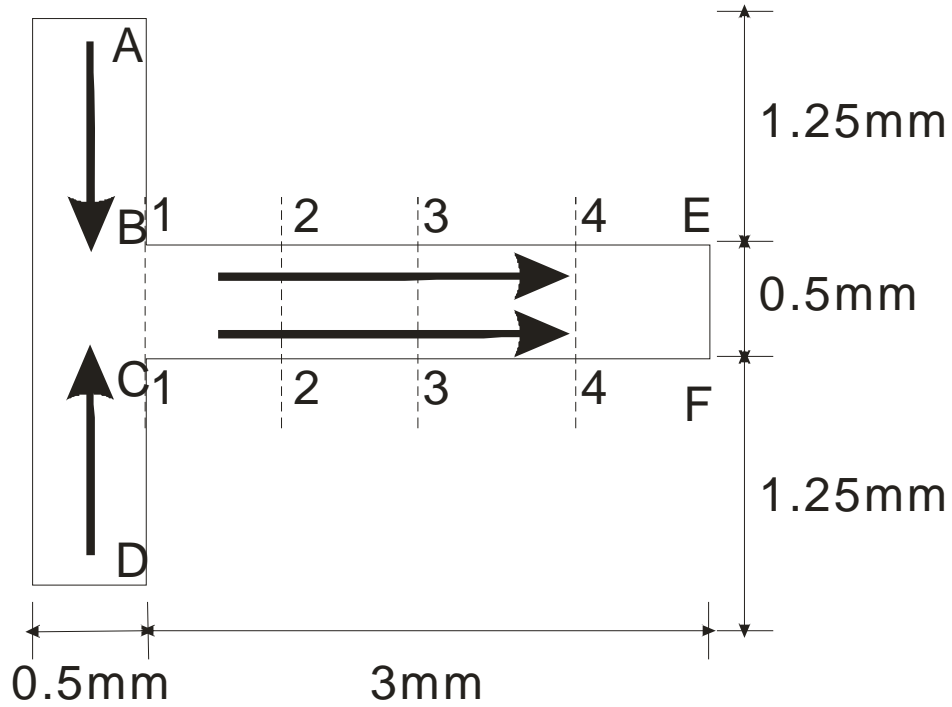
The schematic of the experimental setup for the thermal mixing is shown in Fig. 6. In this experiment, the straight portion of the T-shaped channel has a cross section of  $1000\mu m \times 500\mu m$  and the length of 3 cm. Hot DI-water with Rhodamine B solution (0.025g/100ml) enters the upper inlet arm A-B and cold DI-water with Rhodamine B solution enters the lower inlet arm D-C. Then the two fluids flow side by side in the T-shaped straight microchannel in the direction from BC side to EF side by two identical syringe pumps. Two low voltage power supplies are used to supply voltage to the thermoelectric module to heat up and cool down the Rhodamine B solution in the microchannel.



**Fig. 6 Schematic illustration of experimental setup for thermal mixing**

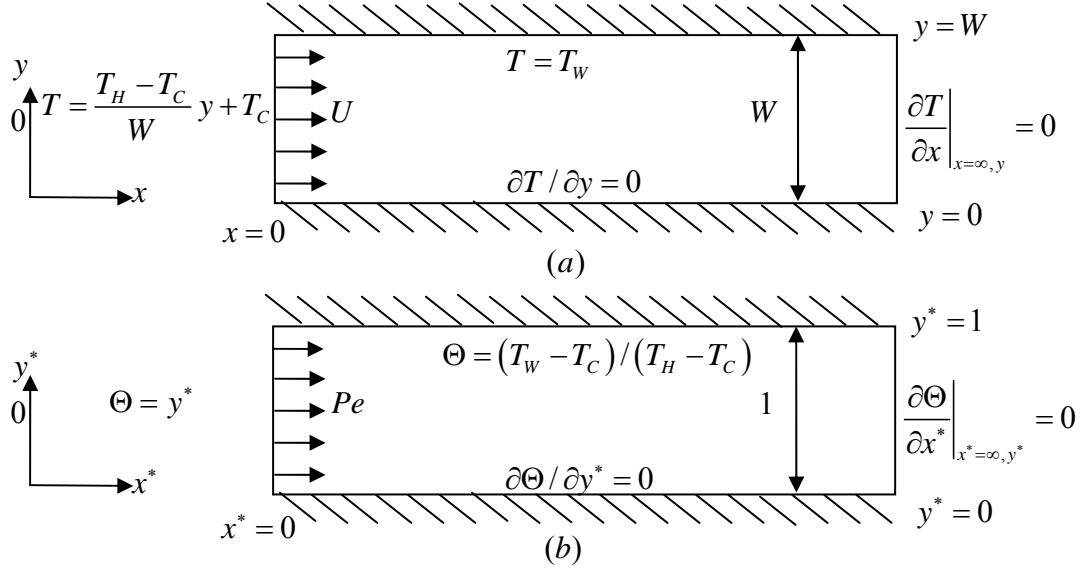
### 3. Theoretical model

Fig. 7 shows the schematic illustration of focused area which is at the intersection of T-shaped microchannel. Hot DI-water enters the channel from upper inlet arm AB. Cold DI-water enters from the lower inlet arm DC. The theoretical model is built along the horizontal area (BCFE) of the T-shaped microchannel.



**Fig. 7 Schematic illustration of focused area captured by CCD camera for thermal mixing**

Fig. 8 illustrates the two dimensional model for the thermal mixing in the microchannel. It is assumed that thermal stratification occurred at the two inlet arms and inlet of the T-junction due to that the diffusion is dominant in vertical regions. Hence, a linear temperature distribution is specified at  $x^* = 0$ . At the upper wall ( $y^* = 1$ ), constant surface temperature is specified due to the thermal conduction from the thermal electric module. At the bottom wall ( $y^* = 0$ ), adiabatic condition is specified due to the little heat loss to the ambient environment. When the channel goes to infinity long ( $x^* \rightarrow \infty$ ), fully thermal mixing will be achieved.



**Fig. 8 Two-dimensional model of thermal mixing in the T-shaped microchannel:**  
**(a) the actual model, (b) the dimensionless model**

In our analysis, the following assumptions are made:

1. Continuum assumption;
2. Two fluids with same property;
3. Decoupled convection and diffusion processes. The process is assumed to occur in a fully developed flow field;
4. The viscosity and thermal diffusivity are independent of temperature;
5. Laminar, incompressible, Newtonian fluid, steady flow is assumed;
6. Convection is assumed to occur in one direction only, axially along the channel.

The governing equation can be formulated in the dimensionless form as:

$$\frac{\partial^2 \Theta}{\partial x^{*2}} + \frac{\partial^2 \Theta}{\partial y^{*2}} = Pe \frac{\partial \Theta}{\partial x^*} \quad (1)$$

The inlet and outlet boundary conditions for Eq. (1) are:

$$\Theta|_{(x^*=0)} = y^* \quad (2)$$

$$\frac{\partial \Theta}{\partial x^*} \bigg|_{(x^* \rightarrow \infty)} = 0$$

The boundary condition for the wall was set as follows:

$$\Theta|_{y^*=1} = (T_w - T_c) / (T_H - T_c) \quad (3)$$

$$\left. \frac{\partial \Theta}{\partial y^*} \right|_{y^*=0} = 0$$

Using the Finite Fourier Transform (FFT) method, and applying corresponding boundary conditions Eq. (2)-(3), we get the dimensionless temperature distribution in the microchannel:

$$\Theta(x^*, y^*) = \sum_{n=1}^{\infty} \left\{ A \exp \left( \frac{Pe^2 - \sqrt{Pe^2 + 4\lambda_n^2}}{2} x^* \right) + \frac{2c(-1)^n}{\lambda_n} \right\} \cos(\lambda_n y) \quad (4)$$

Where  $A = \frac{2(-1)^n}{\lambda_n} (1-c) - \frac{2}{\lambda_n^2}$ ,  $c = (T_w - T_c) / (T_H - T_c)$ .

## 4. Results and discussion

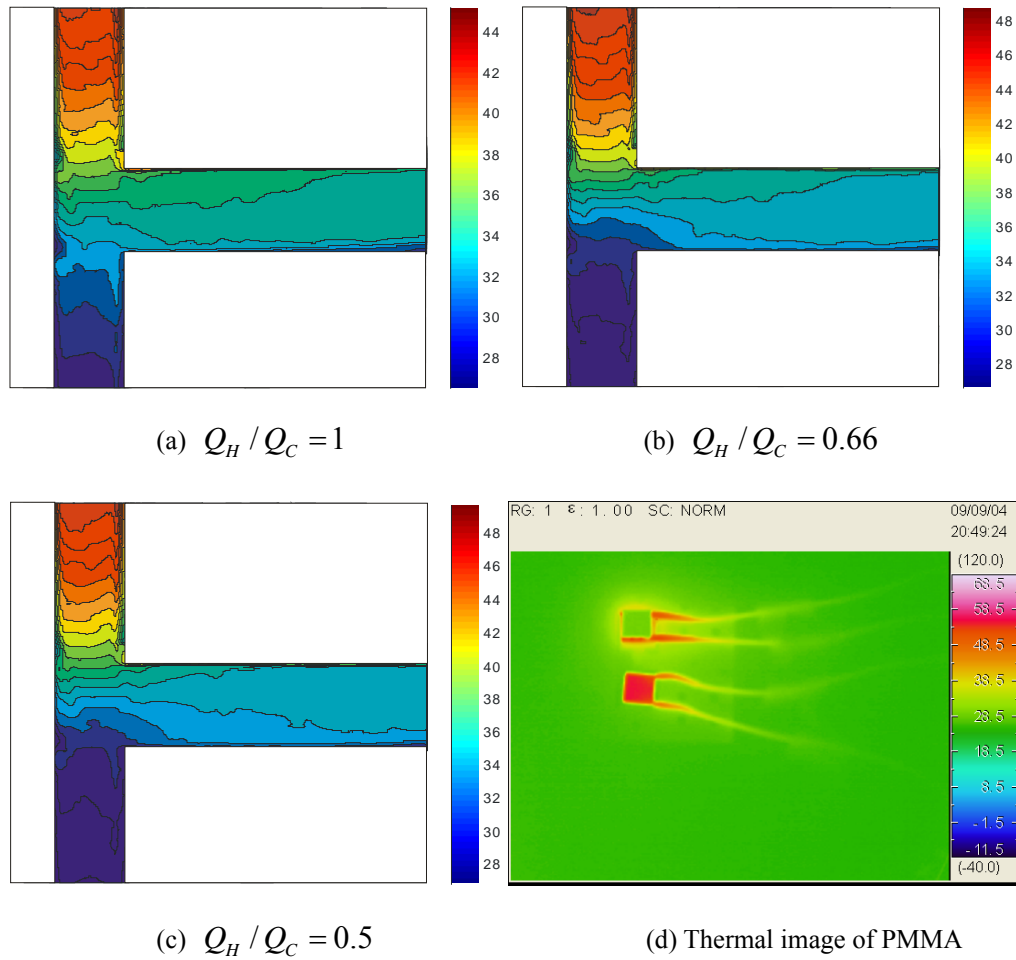
### 4.1. Experimental results and discussion

Fig. 9(a)-(c) shows the measured temperature profiles for three flow rate ratios ( $Q_H / Q_C$ ); 1, 0.66 and 0.5 respectively, of which  $Q_H$  is maintained at  $1000 \mu l / h$ . Hot DI-water with flowrate  $Q_H$  enters the channel from upper inlet arm. Cold DI-water with flowrate  $Q_C$  enters from the lower inlet arm. When  $Q_H / Q_C = 1$ , each stream occupies half of the channel. At the two inlet arms, the temperature contours are stratified, indicating the diffusion is dominant in the inlet arms. The two injected streams meet at the inlet junction (section B-C, Fig. 1) and flow side by side down the main channel. Thermal mixing occurs during the parallel flow through the combined diffusion-convection mechanism. At flow rate ratios of 0.66 (Fig. 8 (b)) and 0.5 (Fig. 9 (c)), the cold stream occupies a larger fraction of the channel as  $Q_C$  increases. Fig. 9(d) shows the typical image captured by the thermal tracer camera.

Fig. 10 shows the temperature distribution along  $y^*$  marked as dotted lines 1-1, 2-2, 3-3 and 4-4, corresponding to  $x^* = 0$ ,  $x^* = 0.25$ ,  $x^* = 0.5$ ,  $x^* = 0.75$  respectively (Fig. 7) when the flowrate ratio is equal to 1. Due to thermal stratification at the two inlet arms, the temperature profile at the inlet junction, 1-1, is not uniform.

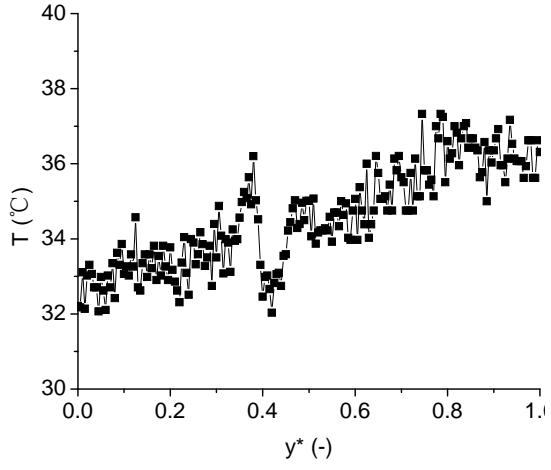
A linear distribution is observed in Fig. 9(a). At  $y^* = 0$  (along C-F), adiabatic boundary condition can be assumed as the cold stream enters the lower inlet arm, of which the temperature is almost the same as ambient condition, so the heat loss along the C-F side is very little. At  $y^* = 1$ , constant surface temperature is assumed due to the thermal conduction from the thermal electric module.

Fig. 11 shows the measured temperature profiles for three flow rate ratios ( $Q_H / Q_C$ ); 1.5, 1 and 0.75 respectively, of which  $Q_H$  is maintained at  $1500 \mu l / h$ ; Fig. 12 shows the measured temperature profiles for three flow rate ratios ( $Q_H / Q_C$ ); 2, 1.33 and 1 respectively, of which  $Q_H$  is maintained at  $2000 \mu l / h$ . These two Figures show the same trend as Fig. 8.

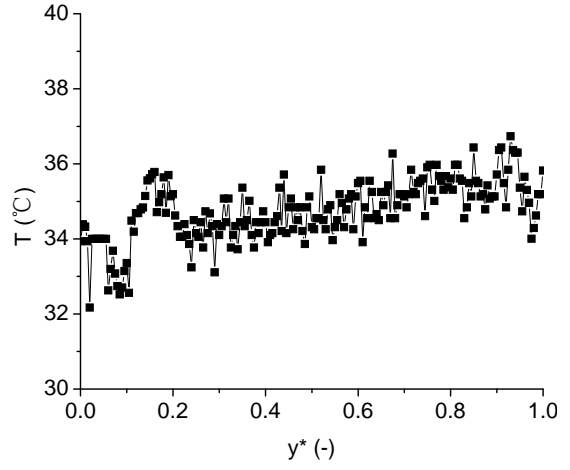


**Fig. 9 Temperature contour plot of T shape thermal mixing and thermal image of PMMA**

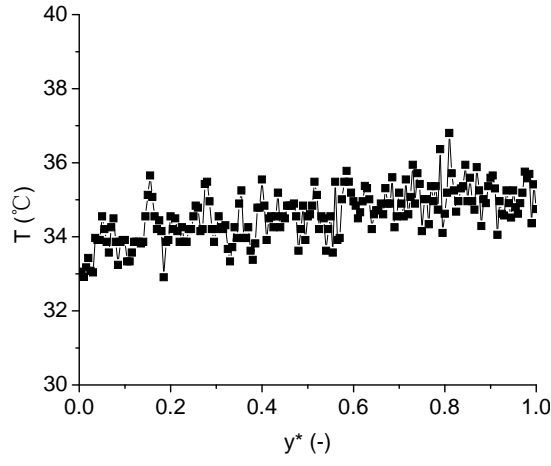
$$(Q_H = 1000 \mu l / h, Q_C = 1000 / 1500 / 2000 \mu l / h)$$



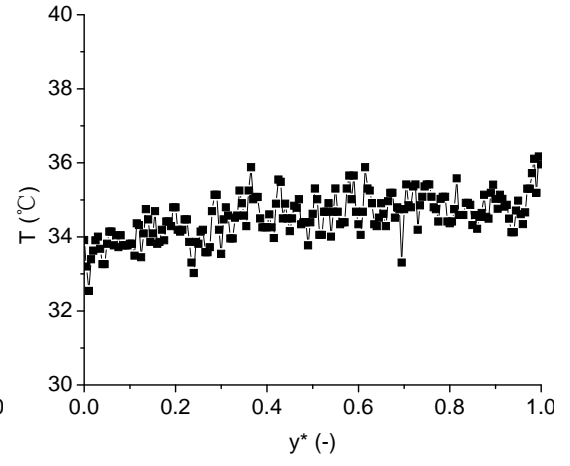
(a)  $x^* = 0$



(b)  $x^* = 0.25$

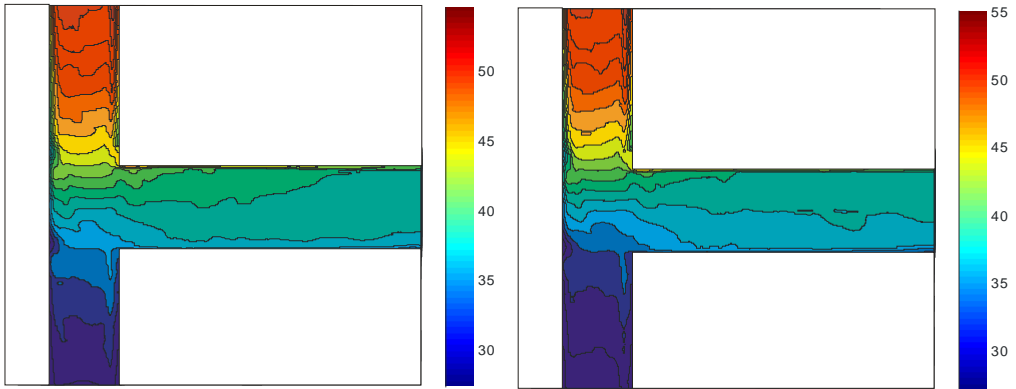


(c)  $x^* = 0.5$



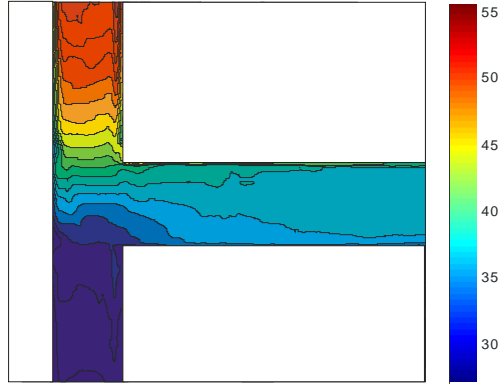
(d)  $x^* = 0.75$

**Fig. 10** Temperature distribution along  $y^*$  at different location ( $Q_H / Q_C = 1$ )



(a)  $Q_H / Q_C = 1.5$

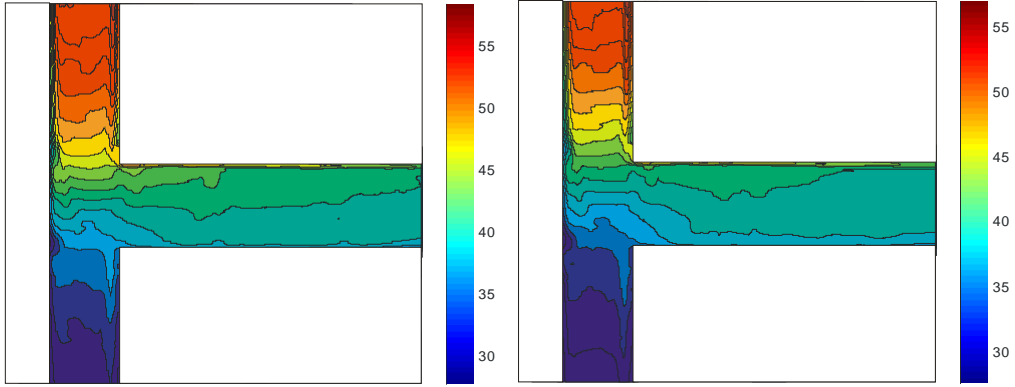
(b)  $Q_H / Q_C = 1$



(c)  $Q_H / Q_C = 0.75$

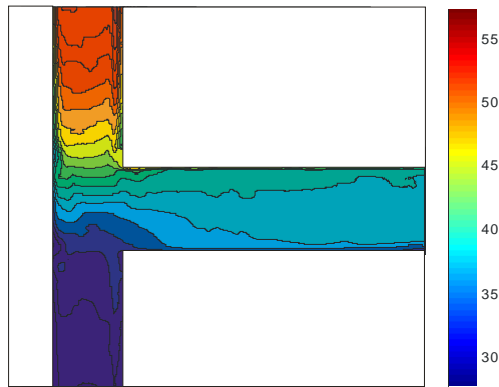
**Fig. 11 Temperature contour plot of T shape thermal mixing**

$(Q_H = 1500 \mu l / h, Q_C = 1000 / 1500 / 2000 \mu l / h)$



(a)  $Q_H / Q_C = 2$

(b)  $Q_H / Q_C = 1.33$



(c)  $Q_H / Q_C = 1$

**Fig. 12 Temperature contour plot of T shape thermal mixing**

$(Q_H = 2000 \mu l / h, Q_C = 1000 / 1500 / 2000 \mu l / h)$

#### 4.2. Comparison between theoretical analysis and experiment result

From Figs. 13-14, we can see that at the entrance region ( $x^*=0$ ), the analytical model agree well with the experimental result. These demonstrate the practicability of the boundary conditions setting for the inlet in the analytical model. It also can be observed that the difference between the analytical and experimental results become larger along the axial direction. This is due to the constant wall temperature boundary condition setting in the analytical model. From experimental result we can see that at the upper boundary, there are heat convection occurred at the boundary. For the analytical model, a constant wall temperature is imposed. So the difference increases along the axial direction.

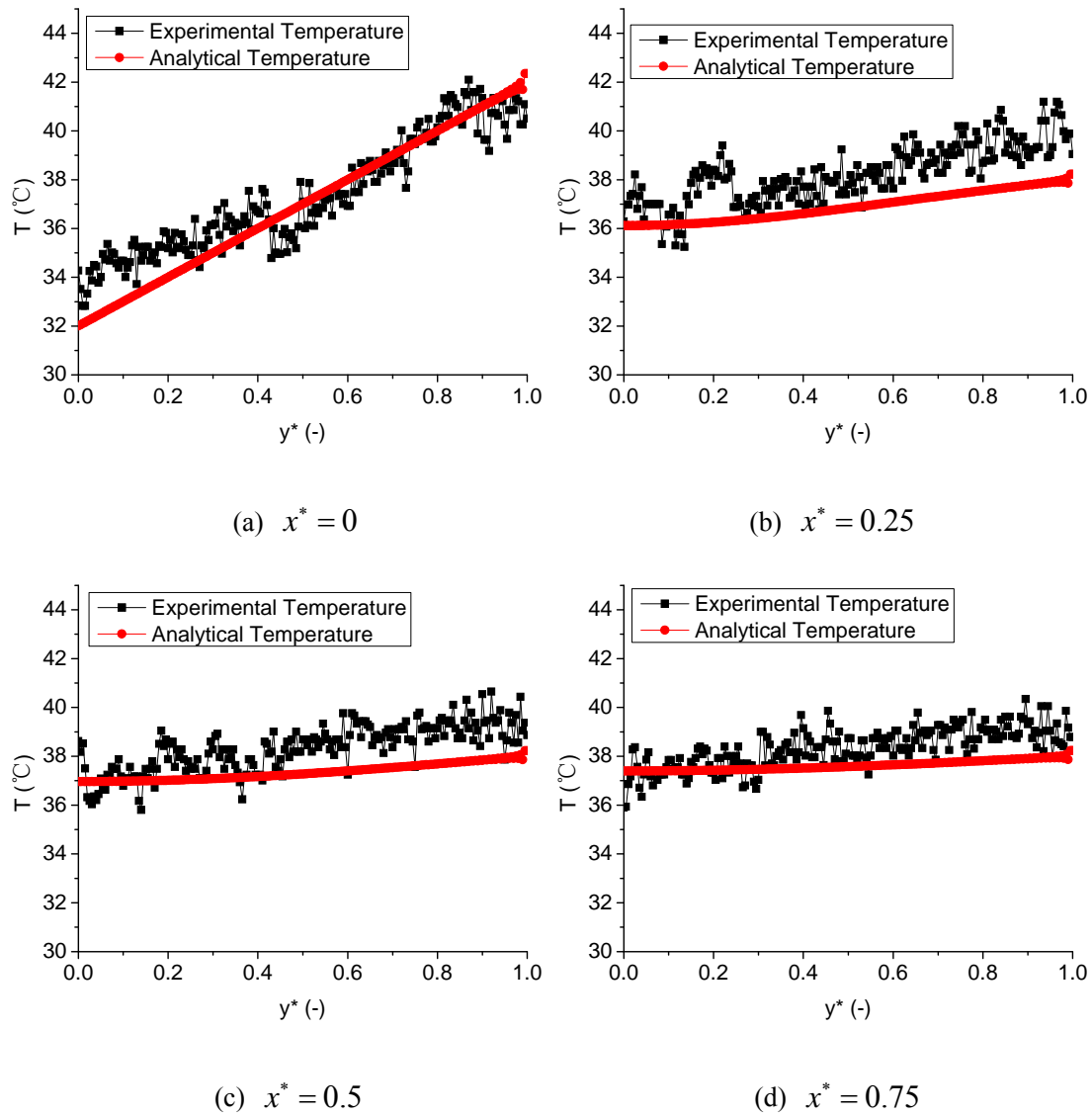


**Fig. 13** Temperature comparison for the flow rate is  $1500 \mu\text{l} / \text{h}$

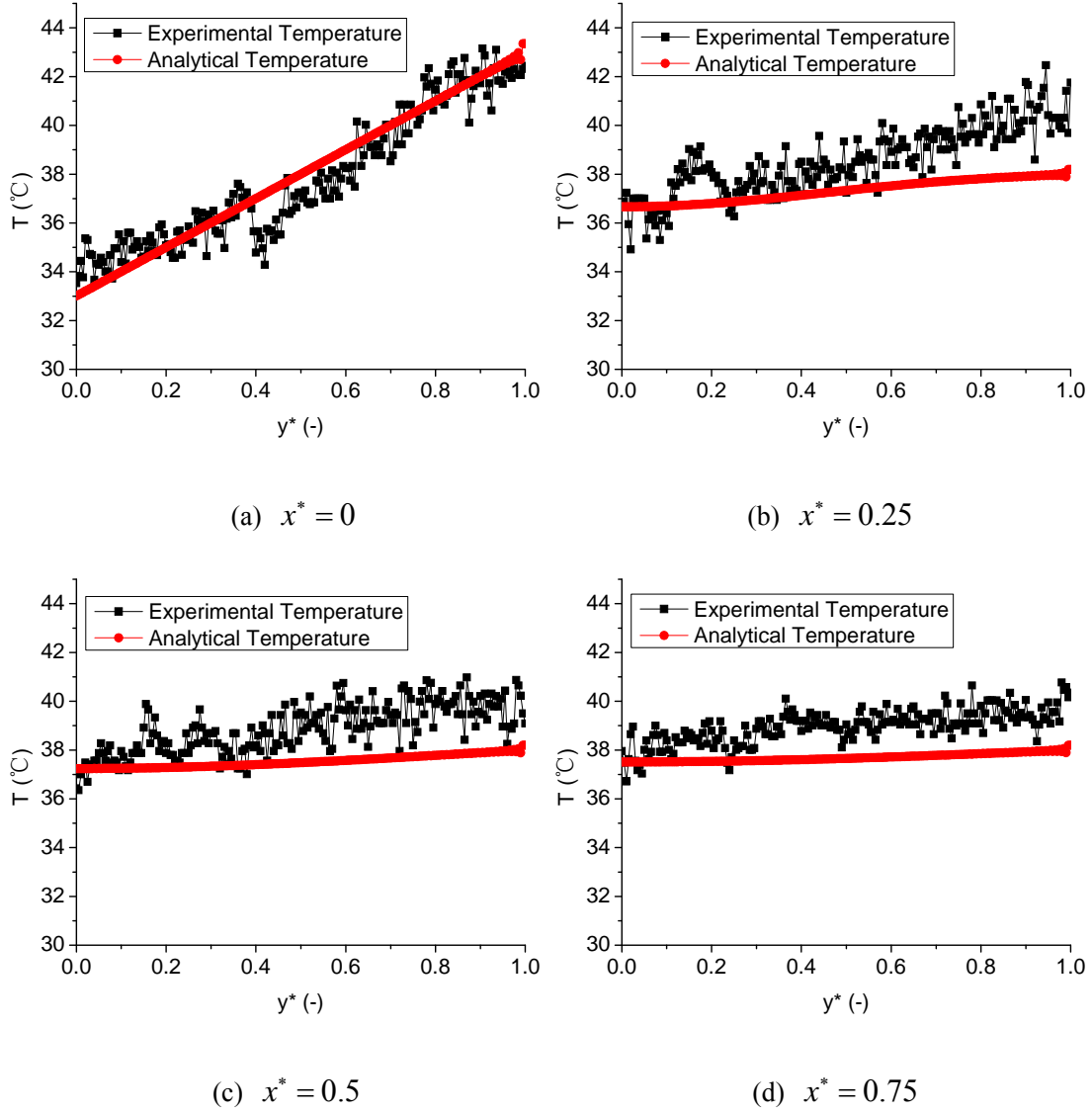


**Fig. 14** Temperature comparison for the flow rate is  $2000 \mu\text{l} / h$

## 5. Conclusions

This paper reports theoretical and experimental investigations for the thermal mixing in the T-shaped microchannel. The internal fluid temperature was measured by the fluorescence imaging technique. The PMMA temperature was captured by the thermal tracer camera. The temperature distributions under different flow rates are investigated. The results indicate that the Reynolds number is a crucial parameter to the heat transfer process in the microchannel. The temperature field changes with different flow rate combinations. The LFID is stratified compared with the mass mixing.

The comparison of the thermal mixing in the T-shaped microchannel between the measured data and the analytical models shows good agreement. The temperature field in the microchannel can be predicted by the theoretical model.

## References

- Auroux, P.-A., D. Iossifidis, D. R. Reyes and A. Manz (2002). "Micro Total Analysis Systems. 2. Analytical Standard Operations and Applications." Analytical Chemistry **74**(12): 2637-2652.
- Chaudhari, A. M. W., T.M.; Albin, M.; Goodson, K.E.; (1998). "Transient liquid crystal thermometry of microfabricated PCR vessel arrays." Journal of Microelectromechanical Systems **7**(4): 345 - 355
- Davis, K. L., K. L. K. Liu, M. Lanan and M. D. Morris (1993). "Spatially resolved temperature measurements in electrophoresis capillaries by Raman thermometry." Analytical Chemistry **65**(3): 293-298.
- Huang, T. and J. Pawliszyn (2002). "Microfabrication of a tapered channel for isoelectric focusing with thermally generated pH gradient." ELECTROPHORESIS **23**(20): 3504-3510.
- Jandik, P., B. H. Weigl, N. Kessler, J. Cheng, C. J. Morris, T. Schulte and N. Avdalovic (2002). "Initial study of using a laminar fluid diffusion interface for sample preparation in high-performance liquid chromatography." Journal of Chromatography A **954**(1-2): 33-40.
- Kamholz, A. E., B. H. Weigl, B. A. Finlayson and P. Yager (1999). "Quantitative analysis of molecular interaction in a microfluidic channel: The T-sensor." Analytical Chemistry **71**(23): 5340-5347.
- Kim, J. A., J. Y. Lee, S. Seong, S. H. Cha, S. H. Lee, J. J. Kim and T. H. Park (2006). "Fabrication and characterization of a PDMS-glass hybrid continuous-flow PCR chip." Biochemical Engineering Journal **29**(1-2): 91-97.
- Lacey, M. E., A. G. Webb and J. V. Sweedler (2000). "Monitoring Temperature Changes in Capillary Electrophoresis with Nanoliter-Volume NMR Thermometry." Analytical Chemistry **72**(20): 4991-4998.
- Liu, K.-L. K., K. L. Davis and M. D. Morris (1994). "Raman Spectroscopic Measurement of Spatial and Temporal Temperature Gradients in Operating Electrophoresis Capillaries." Analytical Chemistry **66**(21): 3744-3750.
- Reyes, D. R., D. Iossifidis, P.-A. Auroux and A. Manz (2002). "Micro Total Analysis Systems. 1. Introduction, Theory, and Technology." Analytical Chemistry **74**(12): 2623-2636.
- Ross, D., M. Gaitan and L. E. Locascio (2001). "Temperature Measurement in Microfluidic Systems Using a Temperature-Dependent Fluorescent Dye." Analytical Chemistry **73**(17): 4117-4123.
- Sommer, G. J., S. M. Kim, R. J. Littrell and E. F. Hasselbrink (2007). "Theoretical and numerical analysis of temperature gradient focusing via Joule heating." Lab on a Chip - Miniaturisation for Chemistry and Biology **7**(7): 898-907.
- Tanaka, Y., M. N. Slyadnev, A. Hibara, M. Tokeshi and T. Kitamori (2000). "Non-contact photothermal control of enzyme reactions on a microchip by using a compact diode laser." Journal of Chromatography A **894**(1-2): 45-51.
- Tomasz Glowacki, Z. A., Shuwen Wang and Carolyn Ren (2009). "Photobleaching absorbed Rhodamine

- B to improve temperature measurements in PDMS microchannels." Journal of The Royal Society of Chemistry **9**: 171-174.
- Wang, J., G. Chen, M. P. Chatrathi and M. Musameh (2004). "Capillary Electrophoresis Microchip with a Carbon Nanotube-Modified Electrochemical Detector." Analytical Chemistry **76**(2): 298-302.
- Wätzig, H. (1992). "The measurement of temperature inside capillaries for electrophoresis using thermochromic solutions." Chromatographia **33**(9): 445-448.